The Company of Biologists

RESEARCH ARTICLE

Sidestep-induced neuromuscular miswiring causes severe locomotion defects in *Drosophila* larvae

Jaqueline C. Kinold, Carsten Pfarr and Hermann Aberle*

ABSTRACT

Mutations in motor axon guidance molecules cause aberrant projection patterns of motor nerves. As most studies in *Drosophila* have analysed these molecules in fixed embryos, the consequences for larval locomotion are entirely unexplored. Here, we took advantage of *sidestep* (*side*)-mutant larvae that display severe locomotion defects because of irreparable innervation errors. Mutations in *side* affected all motor nerve branches and all body wall regions. Innervation defects were non-stereotypical, showing unique innervation patterns in each hemisegment. Premature activation of Side in muscle precursors abrogated dorsal migration of motor nerves, resulting in larvae with a complete loss of neuromuscular junctions on dorsal-most muscles. High-speed videography showed that these larvae failed to maintain substrate contact and inappropriately raised both head and tail segments above the substrate, resulting in unique 'arching' and 'lifting' phenotypes. These results show that guidance errors in *side* mutants are maintained throughout larval life and are asymmetrical with respect to the bilateral body axis. Together with similar findings in mice, this study also suggests that miswiring could be an underlying cause of inherited movement disorders.

KEY WORDS: *Drosophila*, *Sidestep*, Motor axon guidance, Neuromuscular junction, Hydrostat, Larval locomotion

INTRODUCTION

In a highly dynamic and fascinating process, neuronal growth cones migrate through a highly varied cellular environment to find and innervate their target cells. Although embryonic distances are generally relatively short, growth cones contact multiple cell types that express different surface molecules during this period. Growth cones integrate these cues and translate them into steering decisions. One of the largest families of axon guidance molecules is formed by the immunoglobulin superfamily (IgSF). These cell-surface receptors engage in homo- or heterophilic protein-protein interactions, mediating cellular recognition and adhesion processes. Members of this family in *Drosophila*, such as fasciclins (FasI-III), Frazzled (Fra), Uncoordinated 5 (Unc5), Down syndrome cell-adhesion protein (DSCAM), roundabout proteins (Robo1-3), sidestep proteins (Side, SideII-VIII) and beaten paths proteins (BeatI-VII), among others, are involved in axon steering and targeting decisions (Araújo and Tear, 2003; Kolodkin and Tessier-Lavigne, 2011; Zarin et al., 2014b; Li et al., 2017).

Heinrich Heine University Düsseldorf, Functional Cell Morphology Lab, Building 26-12-00, Universitaetsstrasse 1, 40225 Düsseldorf, Germany.

*Author for correspondence (aberle@hhu.de)

H.A., 0000-0002-4864-6105

Mutations in these molecules cause specific motor axon guidance defects that have been categorized as stall, bypass, detour or misroute phenotypes (Lin and Goodman, 1994). Briefly, stalled motor axons project along correct pathways but stop short and fail to probe their target muscles. A bypass arises when motor axons grow beyond their targets, usually because of failures to defasciculate at specific choice points. Detour phenotypes (also called 'reach back') develop when stray growth cones correct their paths and enter the target region from an abnormal direction, resulting in the formation of neuromuscular junctions (NMJs) at uncommon (ectopic) positions. Misrouting occurs when motor axons are diverted to entirely unexpected and abnormal tracks (Lin and Goodman, 1994).

The molecular underpinnings for these phenotypes, however, are only incompletely understood in *Drosophila*, as is the fate and further development of stalled or bypass axons. In one exception, bypass of ventral muscle fields was correlated with hyperinnervation of dorsolateral muscles, but systematic investigations are missing (Sink et al., 2001).

Side is a classical type I transmembrane protein that consists of an N-terminal signal peptide followed by five immunoglobulin domains, a transmembrane domain and a short cytoplasmic domain without known sequence motifs (Sink et al., 2001). It was originally discovered in a large-scale ethyl methanesulfonate (EMS) mutagenesis screen for genes regulating motor axon guidance in *Drosophila* embryos (Sink et al., 2001). Later, it was independently recovered in a larval screen based on a strongly altered innervation pattern (Aberle et al., 2002; Siebert et al., 2009).

Side functions as a target-derived attractant for motor axons, promoting growth along and towards Side-labelled cell surfaces (Sink et al., 2001; Siebert et al., 2009). Mutant phenotypes occur predominantly in the ventral muscle domain, and include a general inability of motor axons to defasciculate from major nerve tracks, with bypass and detour phenotypes being most common (Sink et al., 2001). Consistent with an attractive function, overexpression of Side in wild-type embryos triggers intensive contact and prolonged explorations by neuronal filopodia, even in tissues that are normally ignored by growth cones (Sink et al., 2001). In muscles, this even overturns targeting preferences (de Jong et al., 2005).

Motor axons recognise Side labels via Beaten path Ia (Beat), an IgSF member harbouring two immunoglobulin domains (Siebert et al., 2009). First, *beat* is specifically expressed in motoneurons during the time of axonal outgrowth (Fambrough and Goodman, 1996). Second, *beat*- and *side*-null mutants have highly similar pathfinding phenotypes (Fambrough and Goodman, 1996; Sink et al., 2001). Third, Beat and Side interact biochemically in immunoprecipitation experiments and S2 cell-cell aggregation assays (Siebert et al., 2009). Finally, Side remains constitutively expressed in substrates delineating major motor axon tracks in *beat* mutants, even at the end of embryogenesis, when it is no longer detectable in wild-type embryos using specific antibodies (Siebert et al., 2009).

DEVELOPMENT

1

Together with the spatial distribution of Side-expressing clusters of sensory neurons in the body wall, these findings support the idea that Side functions as a major attractant to steer motor axons towards their dorsal, lateral and ventral muscle fields. Other guidance cues, many of which are expressed in subsets of muscles, such as netrins, Capricious or Connectin, may assist and help to fine-tune steering and targeting decisions (Nose et al., 1994; Mitchell et al., 1996; Shishido et al., 1998; Labrador et al., 2005). Although no orthologs for both Beat and Side have been found in vertebrates, they are highly conserved in arthropods, and the *Drosophila* genome encodes several paralogs that are organized into two protein families (Pipes et al., 2001; Aberle, 2009; Zinn, 2009). Initial analyses of their expression patterns and protein-protein interactions indicate a wider interaction network that might have broader roles in wiring the neuromuscular system and possibly central pathways too (Özkan et al., 2013; Li et al., 2017).

As most studies on *Drosophila* motor axon guidance molecules have been performed during the period of axon growth in fixed embryos, little is known about their postembryonic functions, such as the correction of guidance errors or the consequences for larval locomotion. Accordingly, postembryonic phenotypes have been addressed in only a few studies (Nose et al., 1994; Shishido et al., 1998; Sink et al., 2001; Siebert et al., 2009). As *side* mutants develop into third instar larvae we correlated the final innervation pattern with larval crawling behaviours and searched for noticeable locomotion defects. We found that, on average, 33% of muscle fibres in *side*-mutant larvae permanently lack NMJs containing major type I boutons. In addition, a high percentage of muscle fibres are innervated at ectopic positions in the presence or absence of native innervation. These derangements severely constrain locomotion. Mutant larvae crawl slower and shorter distances, and they are unable to keep firm contact with the substrate, leading to 'arching' phenotypes and unbalanced locomotion, which prevents efficient operation of mouth hooks and ventral denticle belts.

RESULTS
Drosophila embryos form an impenetrable cuticle at the end of embryogenesis. It is for this reason that the final steps in the formation of the neuromuscular system are only rarely assessed. However, motor axons are still dynamic at these stages, undergoing presynaptic differentiation, adjusting trajectories or correcting stalls. To account for these dynamic processes, we aimed for the final innervation pattern in third instar larvae. Because of their large size, even single axons that innervate single muscle fibres are readily distinguishable.

Motor axons in *side* mutants most characteristically fail to defasciculate at a ventral choice point, and grow past their destined muscle fields (Sink et al., 2001; Siebert et al., 2009). However, *side* mutants also show stalled axons and misrouting phenotypes that cannot readily be explained by faulty defasciculation. The intersegmental nerve (ISN), for example, frequently stalls before reaching its dorsal-most muscles or inappropriately grows across segmental boundaries (Sink et al., 2001). To characterize these multifaceted phenotypes at high spatial resolution, we analysed motor axons in ventral, lateral and dorsal body wall regions of intact animals (Fig. 1A,B).

Mutations in *side* affect all body wall regions
We expressed the red fluorescent protein dsRed in motoneurons using OK371-Gal4 in the background of the postsynaptic marker Shaker-GFP (ShGFP, also called CD8-GFP-Sh). At the dorsal-most choice point, the ISN splits into an anterior and posterior branch to innervate muscle (M) 1 and M9 (Fig. 1C,D). In *side* mutants, either

one or both of these muscles frequently lacked NMJs (Fig. 1E, Table 1). Embryonic stalls in the posterior branch of the ISN caused a similar lack of the distal-most synaptic ending in this pathway: the NMJ on M18 (Fig. 1E, see also Fig. 1H and Table 1). On average, at least one terminal NMJ was lacking in the dorsal muscle field (quantified in Fig. 4J; see Materials and Methods for definition of muscle fields).

In the lateral muscle field (Fig. 1F), highly variable detour and stall phenotypes were most prominent. For example, axons normally migrating in the segmental nerve SNa erroneously defasciculated from the ISN at lateral levels (compare arrowheads in Fig. 1G and H). Distal-most muscle M24 frequently lacked innervation (arrows in Fig. 1G,H, Table 1). To a lesser extent, NMJs on M21 or M5/8 were also missing (Fig. S1, quantified in Fig. 4J). In the ventral muscle field (Fig. 1I), we predominantly identified bypass and detour phenotypes, easily recognized by the lack of NMJs and nerve branches in this region (compare arrowheads in Fig. 1J and K). Most axons continued to grow along the ISN, but subsets of them managed to innervate ventral muscles by detours, sprouting short branches directly out of the ISN (arrow in Fig. 1K). Note that bypassing axons remained fasciculated with the ISN, rendering it much thicker at the level of M12 [7.4 ± 1.6 μm (mean±s.d.) in $side^{C137}/side^{I1563}$ ($n=11$) compared with 3.3 ± 0.6 μm in ShGFP control larvae ($n=15$)] (Fig. 1J, K). Thus, mutations in *side* cause innervation errors in ventral, lateral and dorsal body wall regions, and all four classes of embryonic projection errors can be detected in larvae.

Asymmetrical and unilateral innervation in *side* mutants
The positions of NMJs at identified muscle fibres are normally highly stereotypical in wild-type larvae. One might therefore expect that mutations in a single gene cause reproducible mismatches and affect each muscle fibre in a predictable manner, e.g. NMJs on M12 are always missing. However, *side*-mutant larvae showed noticeable irregularities and asymmetries in the innervation pattern.

We therefore compared motor axon projections along and across the bilateral body axis (Fig. 2). In dorsal views of ShGFP control larvae, NMJs were distributed in a symmetrical pattern in abdominal segments A3 and A4 (Fig. 2A). In *side* mutants, however, innervation of dorsal-most muscles was not stereotypical. For example, NMJs were present in A3 but lacking in a hemisegment of A4 (arrowhead in Fig. 2B). In ventral views, NMJ patterns were similarly irregular along the anterior-posterior axis (arrowhead in Fig. 2D). When we compared innervation across the midline, motor nerve projections were highly asymmetrical between left and right hemisegments, frequently leading to unilateral innervation (vertical arrows in Fig. 2B,D). The extent of randomness and one-sidedness could occur in any abdominal segment. Thus, in *side*-mutant larvae, we observed guidance errors in every hemisegment, but the kind of defects varied between hemisegments.

This is also reflected in the total number of NMJs per hemisegment. Whereas ShGFP control larvae contained, on average, between 26 and 30 NMJs per abdominal hemisegment, the number varied between nine and 25 NMJs in *side* mutants (Table 2). The extreme qualitative and quantitative variations indicate that pathfinding decisions seem to be made rather independently in each hemisegment.

Overexpression of Side in myoblasts deviates motor axons into undifferentiated muscle fields
At the end of embryonic development, endogenous Side is expressed at low levels in differentiated muscle fibres (Sink et al., 2001; Siebert et al., 2009). It is not visibly expressed in muscle
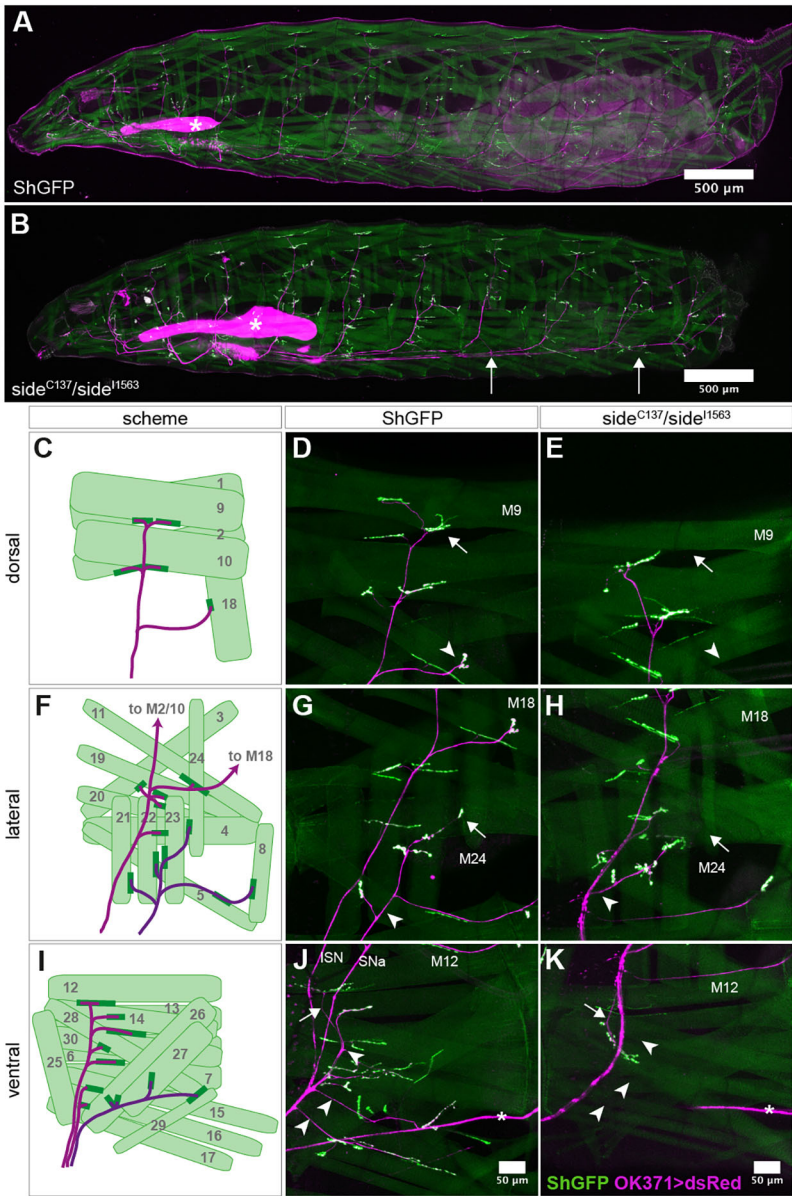
Fig. 1. Motor axon guidance and innervation errors occur in all body wall regions of *side*-mutant third instar larvae. (A,B) Confocal micrographs (projections) acquired through the translucent cuticle of undissected ShGFP (A) and *side*-mutant (B) larvae expressing the postsynaptic marker ShGFP (green) in muscles and the red fluorescent protein dsRed in motor axons and salivary glands (magenta). Two hemisegments lacking the most ventral NMJs are highlighted by arrows in *side* mutants. Asterisks indicate salivary glands. (C-E) Schematic innervation pattern of dorsal muscles as specified in the Materials and Methods (C), with projections of confocal images of the corresponding region in ShGFP (D) and *side* mutants (E), showing a failure to innervate M9 (compare arrows). The branch to M18 is also not developed (arrowheads). (F-H) Schematic of the lateral muscle field, with the SNa pathway marked in dark magenta (F). Confocal images of ShGFP (G) and *side* mutants (H) displaying detour and stall phenotypes. Axons normally projecting via the SNa erroneously exit the ISN (compare arrowheads in G and H) and the distal-most muscle M24 lacks NMJs (compare arrows in G and H). (I-K) Schematic of the ventral muscle field (I) and images of ShGFP (J) and *side* mutants (K) depicting absence of the ISNb, SNc and ISNd branches and their NMJs (compare arrowheads in J and K). Some ventral axons make a detour via the ISN (compare arrows in J,K). Asterisks mark irrelevant segmental nerves. Genotypes: w; OK371-Gal4/+; ShGFP UAS-dsRed in A,D,G,J; w; OK371-Gal4/+; ShGFP *side*[C137]/ShGFP *side*[I1563] UAS-dsRed in B,E,H, K. Scale bars: 500 µm in A,B; 50 µm in J,K.

progenitors (myoblasts, founder cells). From a mechanistic view, this is interesting, because outgrowing motor axons have to transverse myogenic tissues, in which myoblasts fuse with muscle founder cells (Weitkunat and Schnorrer, 2014; Dobi et al., 2015). As myoblasts are highly motile and constantly change positions or disappear by fusion, it would probably 'confuse' growth cones if these cells were expressing attractive cues. However, using Myocyte enhancer factor 2 (Mef2)-Gal4, which is highly active in these precursors, it is possible to ectopically express guidance cues prematurely. When we used Side as an attractant, we could reprogram guidance preferences. Motor axons were prominently attracted to myoblasts and differentiating myotubes (Fig. 3).

At stage 14, ISN growth cones of ShGFP control embryos reached similar dorsolateral positions (Fig. 3A′). This regular growth was no longer observed when exogenous Side was under the control of Mef2-Gal4 (Fig. 3B′,C′). Attraction to, and interaction with, motile myoblasts likely misdirected growth cones, causing irregular migration fronts. Although these phenotypes were most prominent dorsal to the lateral bidendritic neuron (LBD, arrowhead in Fig. 3A), misprojections also occurred in regions ventral to it (arrow in Fig. 3C′).

As expression of ShGFP starts at stage 15, tight interaction with muscle precursors was more visible at stage 16. Although the ISNs synchronously reached their dorsal-most positions in ShGFP

Table 1. Innervation of specific muscles in control and *side*-mutant larvae, using ShGFP for NMJ identification

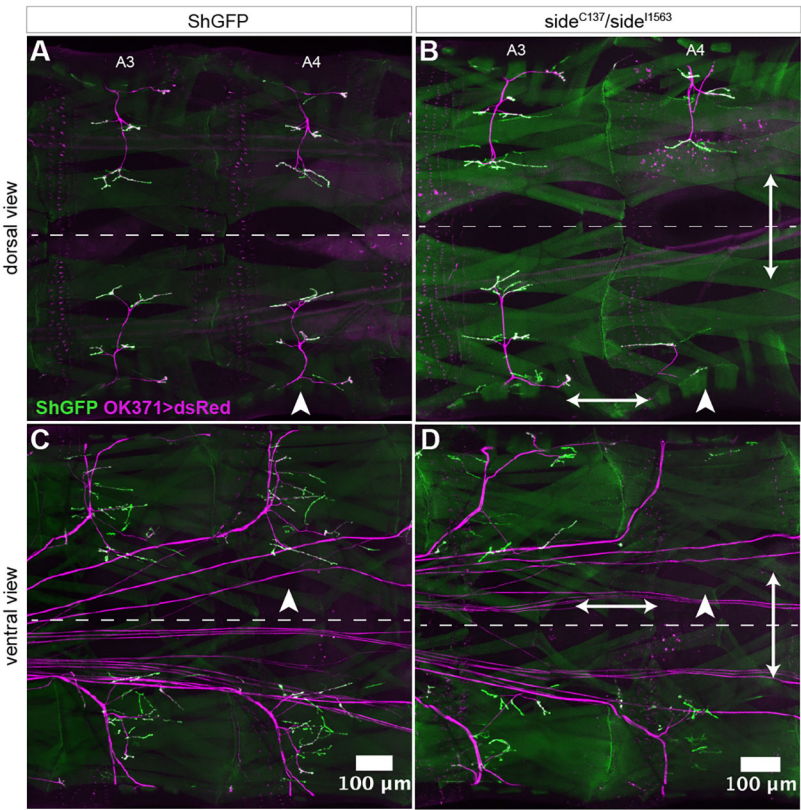| Muscle fibre		1	9	2	10	18	4	21	22	23	24	5	8	12	13
Innervation (%)	ShGFP	100	100	100	100	100	100	100	100	100	100	100	100	100	100
	side[C137]/*side*[I1563]	83	73	93	87	50	97	87	97	97	43	80	83	57	43

n=30 muscles

Fig. 2. Asymmetrical and hemisegment-specific innervation errors in *side* mutant-larvae. (A-D) Confocal micrographs (projections) of two adjacent abdominal segments (A3-A4) of intact third instar larvae expressing ShGFP in muscles (green) and dsRed in motor axons (magenta). Dashed lines indicate the body midline. (A,C) Dorsal (A) and ventral (C) views of ShGFP control larvae showing stereotypical and symmetrical innervation patterns. Arrowheads mark innervated hemisegments. (B,D) Dorsal (B) and ventral (D) views of *side*-mutant larvae exhibiting non-stereotypical and asymmetrical innervation along the anterior-posterior axis (double-headed horizontal arrows) and across the midline (double-headed vertical arrows). Arrowheads mark barely innervated hemisegments. Genotypes: w; OK371-Gal4/+; ShGFP UAS-dsRed in A,C; w; OK371-Gal4/+; ShGFP *side*[C137] /ShGFP *side*[I1563] UAS-dsRed in B,D. Scale bars: 100 µm.

controls (Fig. 3D′), they were highly irregular and mostly stalled in lateral positions in Side-overexpressing embryos (Fig. 3E′,F′). Growth cones were also much larger and frequently bifurcated in opposite directions, which is usually not seen in wild-type embryos (arrows in Fig. 3E′). Expression of full-length Side tagged with mCherry at its C terminus (Side-Cherry) showed even stronger premature stalls (Fig. 3F′). Phenotypic strength was generally increased in Side-Cherry animals, which correlated well with increased Side-Cherry mRNA levels detected by qPCR (data not shown). We also expressed Side and Side-Cherry in a single muscle fibre (M12) in an otherwise wild-type background using 5053-Gal4. This caused supernumerary NMJs on M12 and neighbouring M13 but not on other muscles (Fig. S2K-M), underscoring the attractive function of Side.

Premature stalls of the ISN prefigure absence of dorsal NMJs in larvae

Despite the severe guidance phenotypes, Side-overexpressing embryos develop into third instar larvae. We therefore tried to determine whether stalled growth cones eventually manage to innervate their target muscles. When we examined third instar ShGFP larvae overexpressing Side or Side-Cherry under control of Mef2-Gal4, we found that up to 65.8% or 95.2% of NMJs in the dorsal muscle field were completely missing, respectively,

indicating that stalled and distracted ISN growth cones never reached them (Fig. 4A,D,G, quantified in J). We tested a variety of axon guidance molecules in this overexpression assay, including those with well-known attractive or repulsive functions, such as netrins, fasciclins or semaphorins, among others, but none of them exerted a similar devastating effect on dorsal innervation, suggesting that Side is one of the strongest attractants in *Drosophila* (Fig. S2). Thus, muscle overexpression followed by assessing dorsal NMJs could serve as an assay to quantify attractive strengths of motor axon guidance molecules.

In the ventral muscle field, however, we did not find an increase in the total number of NMJs, but did detect supernumerary NMJs at a subset of muscle fibres, particularly M12 and M13. For example, M12 carried up to three ShGFP-stained NMJs, two of them at ectopic sites (Fig. 4C,F,I). The NMJs appeared also somewhat smaller and less branched, indicating that Side might also regulate NMJ structure. We quantified the total number of NMJs in larvae overexpressing upstream activation sequence (UAS)-Side or UAS-Side-Cherry and found that they were reduced, on average, by 19% and 34%, respectively (Fig. 4J). In comparison, *side* mutants lost 33% of NMJs (Fig. 4J). Thus, Side gain- and loss-of-function mutants had a comparable number of total NMJs per hemisegment but, depending on genotype and attractiveness, NMJs are either predominantly absent on dorsal or on ventral muscles.

Table 2. Range of the total number of NMJs in an entire abdominal hemisegment (%) in the indicated genotypes

Number of NMJs per hemisegment	9	10	11	12	13	14	15	16	17	18	19	20	21	22	23	24	25	26	27	28	29	30
ShGFP (n=42)	0	0	0	0	0	0	0	0	0	0	0	0	0	0	0	0	0	10	10	26	31	24
side[C137]/*side*[I1563] (n=42)	2	0	0	2	0	4	6	4	13	13	10	10	8	6	13	6	2	0	0	0	0	0
mef2>Side[29A] (n=52)	0	0	0	0	0	0	2	2	2	4	8	4	8	8	12	15	12	15	2	6	2	0
mef2>Side-Cherry (n=45)	0	0	0	0	2	0	9	9	18	9	13	16	4	11	2	4	2	0	0	0	0	0

For example, *side*[C137]/*side*[I1563] mutants had 2% of hemisegments with only 9 NMJs. n, number of hemisegments scored.
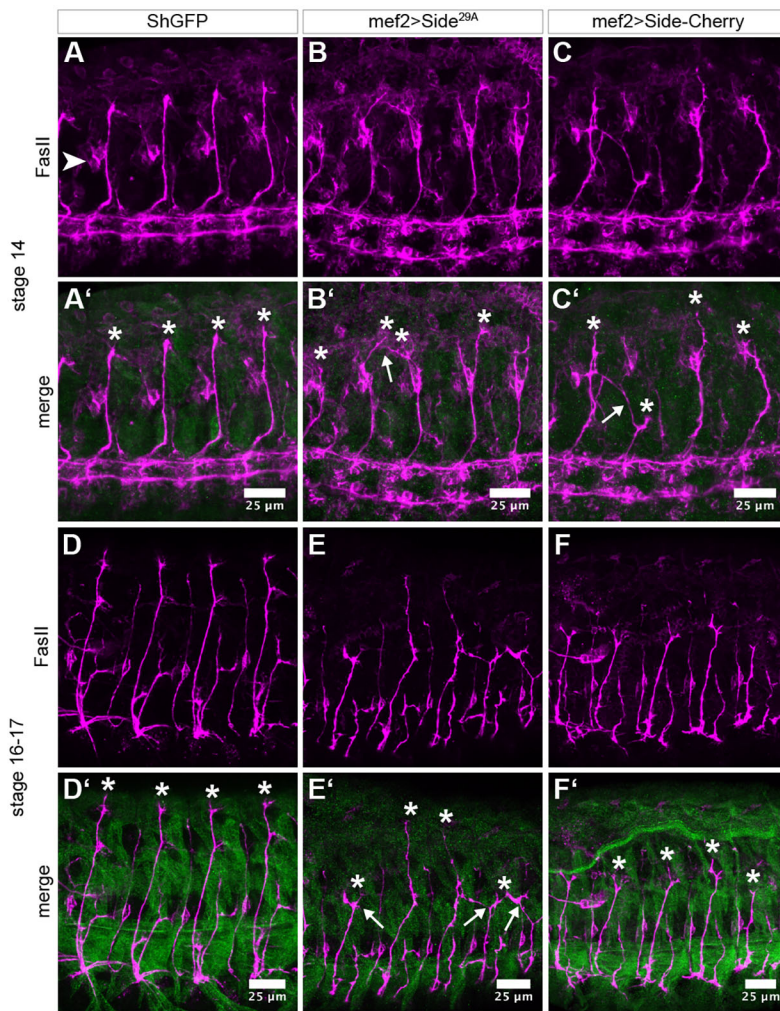
Fig. 3. Overexpression of Side in muscle progenitors prematurely attracts motor axons into developing muscle fields. (A-C) Confocal micrographs (projections) of ShGFP control, Side- and Side-Cherry-overexpressing embryos (stage 14) stained with anti-FasII (magenta) to reveal motor axons. Arrowhead in A marks a representative LBD neuron. (A′-C′) ShGFP in the background of all genotypes stained with anti-GFP and merged with the FasII signal. ShGFP stains only weakly at this stage. Arrows mark misrouted ISNs dorsal and ventral to the LBD. (D-F) Stage 16 embryos of the same genotypes stained with anti-FasII (magenta). (D′-F′) Merged images of ShGFP and FasII signals. Arrows mark bifurcated ISN growth cones in tight contact with developing myotubes. Asterisks in A′-C′ and D′-F′ mark dorsal-most ISN growth cones, usually regular in controls and highly irregular in embryos overexpressing Side. Genotypes: w;; ShGFP in A,A′,D,D′; w;; UAS-Side^{29A}/ mef2-Gal4 ShGFP in B,B′,E,E′; w; UAS-Side-Cherry/+; mef2-Gal4 ShGFP/+ in C,C′,F,F′. Scale bars: 25 µm.

Lack of NMJs on dorsal-most muscles induces body shape changes

During handling of these larvae for microscopy we noticed that immobilization by brief submersion in hot water (1 s, 60-65°C) (Aberle et al., 2002) forced overexpressing larvae into a peculiar crescent shape (Fig. 5C,D), whereas control animals remained straight (Fig. 5A). To examine possible reasons for this shape change, we used UAS-Side-Cherry/+; mef2-Gal4/+ larvae. These larvae were somewhat smaller but exhibited the strongest phenotype, lacking innervation on most, if not all, dorsal muscle pairs 1/9 and 2/10 (Fig. 5D). In contrast to our expectations, the dorsal side appeared to be under greater tension than the almost round ventral side (Fig. 5D). The diameters of dorsal muscles M9 and M10 were on average also thicker in Side-Cherry larvae compared with controls (Fig. 6A, quantified in Fig. 6B), and they were also shorter than ventral muscles M12 or M13 in the very same hemisegment (Fig. 6C).

In contrast, *side*-mutant larvae, in which NMJs are predominantly lacking on ventral muscles, were rather straight with a slight downward curvature (Fig. 5B). Morphometric analysis confirmed that M12 and M13 were shorter on average than dorsal muscles M9 and M10 in the same hemisegment (Fig. 6C). It thus appears that heat-shock-induced deaths curve larval bodies towards non-innervated sides.

To examine whether this could also be observed in living animals, we examined larvae overexpressing Side-Cherry in muscles for locomotion and behavioural phenotypes. These larvae displayed already conspicuous behaviours in food vials, as they had difficulties in climbing the walls and frequently pupated on the food. To measure larval locomotion speed, we transferred first instar larvae (28-36 h after egg laying) to fruit agar plates and quantified the distances crawled in a 10 min time interval (Fig. 5E). Larvae overexpressing Side made less progress and reached only about half the velocity of controls [3.3±1.6 mm/min for UAS-Side-Cherry/+; mef2-Gal4/+ (n=20) versus 5.1±2.0 mm/min for ShGFP (n=19)] (Fig. 5E,F). Similar results were obtained for third instar larvae in a 1 min time interval (22.3±4.1 mm/min for UAS-Side-Cherry/+; mef2-Gal4/+ (n=22) versus 41.1±13.8 mm/min for ShGFP, (n=23)] (Fig. 5E,F). Thus, reduced locomotion correlates with alterations in the wiring pattern.

Errors in the neuromuscular wiring cause larval locomotion defects

Next, we placed control and *side*-mutant third instar larvae on apple juice plates and observed their crawling behaviour using a high-speed video camera. Forward locomotion is normally initiated at the posterior end and consists of a wave of peristaltic contractions progressing towards the head region (Roberts, 1971; Green et al., 1983; Berrigan and Pepin, 1995). The cycle starts with contractions in the terminal segments (A8-A9) that lift the tail off the substrate, move it forward and replant it more anteriorly. This triggers a segment-to-segment peristaltic wave of muscular contractions that slides in an anterior direction over visceral tissues
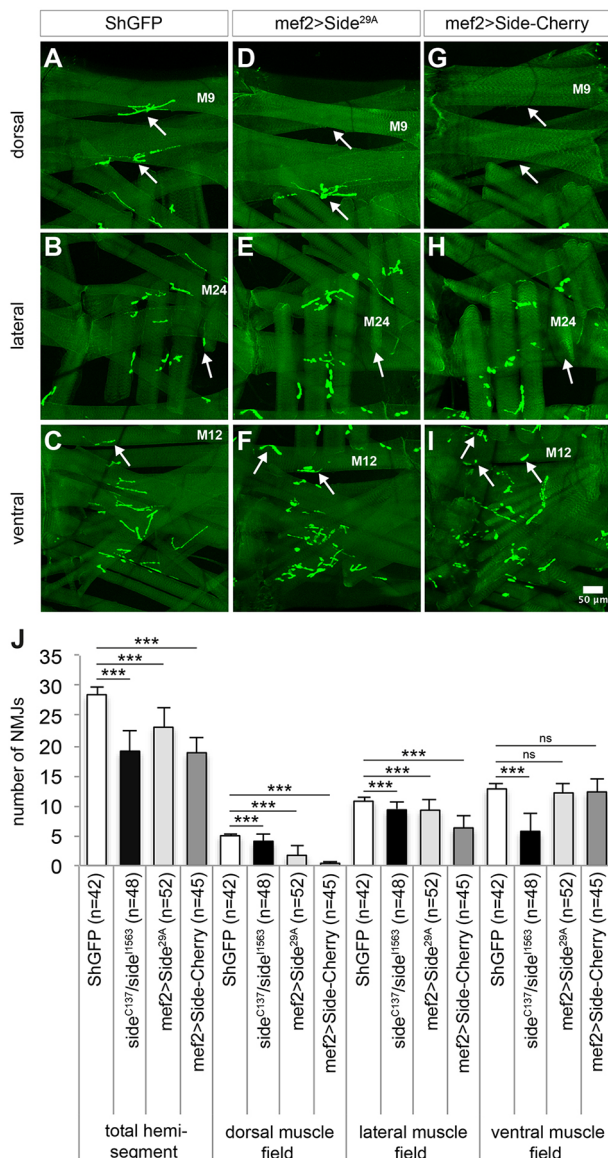
Fig. 4. Premature attraction into embryonic muscle fields prevents innervation of dorsal-most muscles in larvae. (A-I) Confocal micrographs (projections) depicting the neuromuscular innervation pattern marked by ShGFP in dorsal, lateral and ventral regions of third instar larvae. (A-C) ShGFP control larvae showing innervation of dorsal-most muscle pairs M1/9 and M2/10 at central positions (arrows in A), of lateral muscle M24 at a ventral location (arrow in B) and of ventral muscle M12 at a ventral-anterior position (arrow in C). (D-F) Larvae overexpressing untagged Side in muscles frequently lack NMJs on dorsal-most (D) and distal-most (E) muscles. In contrast, a subset of ventral muscles carries supernumerary terminals (e.g. M12, arrows in F). (G-I) Overexpression of Side-Cherry causes highly similar but stronger phenotypes, particularly on dorsal muscles (arrows in G). (J) Quantification of the total number of NMJs stained with ShGFP in larvae of the indicated genotypes and body wall regions. Overexpression of Side-Cherry strongly reduces the number of dorsal NMJs. ***$P<0.001$ (Statistical significance calculated using two-tailed Mann–Whitney U-test, compared with ShGFP control larvae). Data are mean±s.d. n, number of hemisegments; ns, not significant. Genotypes: w;; ShGFP in A-C; w;; UAS-Side[29A]/mef2-Gal4 ShGFP in D-F; w; UAS-Side-Cherry/+; mef2-Gal4 ShGFP/+ in G-I. Scale bar: 50 μm.

(Wang et al., 1997; Heckscher et al., 2012). Once the wave arrives in the head region, the larva raises its head, extends it anteriorly and attaches the mouth hooks to the substrate, which serve as an anterior anchor point (Dixit et al., 2008).

Crawling speed usually ranges between 0.7 and 1.1 mm/s on agar or agarose substrates at room temperature (Berrigan and Pepin, 1995; Wang et al., 1997; Ainsley et al., 2003; Suster et al., 2003). Stride length, the progress made by each contraction cycle, typically varies between 0.6 and 1.8 mm, and stride frequency varies between 0.7 and 1.7 contraction cycles per second (Berrigan and Pepin, 1995; Wang et al., 1997; Risse et al., 2013). Under our conditions (room temperature, 2% agarose substrate), crawling speeds reached, on average, 0.7±0.2 mm/s (n=23) in ShGFP larvae, and an average contraction wave lasted for 0.9±0.2 s (n=20) (data are mean±s.d.) (Fig. 7A-L, Movies 1 and 5). Importantly, contact with the substrate was never visibly lost during progression of the peristaltic wave, as has previously been observed (Dixit et al., 2008).

In marked contrast, *side*-mutant larvae obviously detached from the substrate for extended periods, resulting in 'arch-like' figures and 'inchworm-like' behaviours (Fig. 7A′-L′, Movie 2). They also excessively raised their head and tail segments. Average contraction waves were slower (1.2±0.4 s, n=19), reducing crawling speeds to 0.6±0.2 mm/s (n=26). On average, we failed to detect left-right asymmetries during the contraction waves, despite irregular hemisegmental innervation. However, *side*-mutant larvae that lacked innervation on ventral muscles in three to four consecutive segments on one side of the body, but not on the other side, showed asymmetrical contraction waves, visible as kinks and bends in the body wall (Fig. S3), similar to those observed after complete denervation of single hemisegments (Heckscher et al., 2015).

Larvae overexpressing untagged Side in muscles showed an even more pronounced crawling phenotype, with stronger head and tail lifting and body wall 'arching' (speed 0.5±0.2 mm/s, contraction wave 0.9±0.2 s, n=22) (Fig. 7A″-L″, Movie 3). Consistent with decreased dorsal innervation, Side-Cherry-overexpressing larvae raised their head and tail segments not only more drastically, but also simultaneously (Fig. 7A‴-L‴, Movie 4). Crawling speeds were only 0.4±0.1 mm/s (n=22). These larvae also showed the highest degree of 'unbalanced' locomotion, which is likely to be the compensatory movement that we observed in dorsal views and that resulted in bending along the longitudinal axis, combined with rolling to the left or to the right (Table 3, Movie 6). Of note, the peristaltic wave seemingly progressed without interruption, even on the dorsal side, indicating that non-innervated muscles are not completely stiff but are still able to react to ventral contractions (Movies 4 and 6). Thus, even in the absence of one-third of all NMJs, and regardless of whether they are lacking on ventral or dorsal muscles, incorrect wiring is compatible with larval locomotion, but reduces crawling speeds and induces peculiar compensatory movements.

DISCUSSION

We examined the final outcome of embryonic motor axon guidance errors on the positions of NMJs and larval crawling behaviour. Manipulations of Side caused severe innervation defects in all body wall regions. Importantly, the lack of NMJs was permanent and could not be corrected over time.

Side has previously been shown to function as a target-derived attractant for motor axons (Sink et al., 2001; de Jong et al., 2005; Siebert et al., 2009). As the ISN grows in a straight path from the ventral nerve cord to its dorsal targets, and is later joined by the ISNb and ISNd nerves (ISNb/d), which innervate ventral muscles, the lack of NMJs in both ventral and dorsal regions in *side* mutants could be explained by the loss of a substrate-bound attractant. Indeed, it has been discussed that mesodermal tissues in ventral regions might play an instructive role in defasciculation
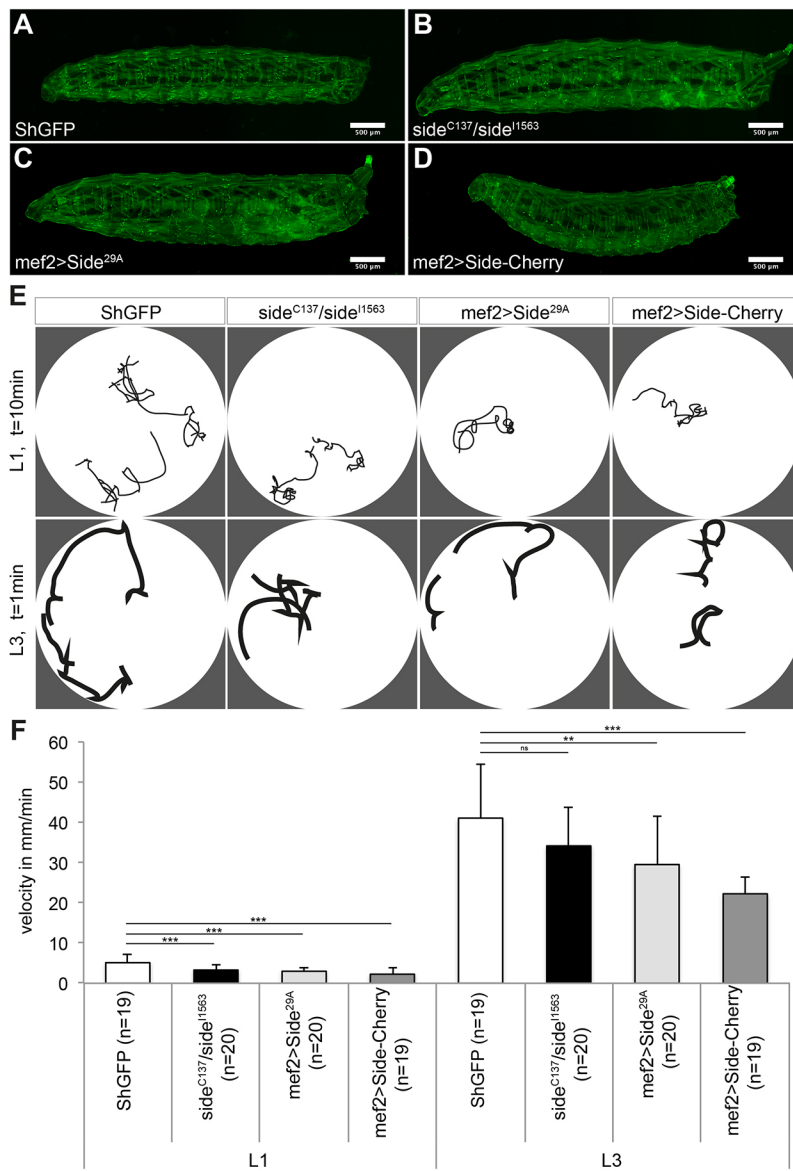
Fig. 5. *Drosophila* larvae lacking dorsal NMJs are associated with crescent-shaped postures and crawl slower. (A-D) Stitched confocal image stacks of third instar larvae expressing ShGFP in the background of the indicated genotypes. Whereas *side* mutants predominantly lack NMJs on ventral muscles, larvae overexpressing Side lack them mostly on dorsal muscles. (E) Schematic tracks of first (L1) and third (L3) instar larvae crawling on fruit agar plates for 10 min and 1 min, respectively. (F) Average crawling velocities of L1 and L3 on fruit agar plates. The loss of *side* or the overexpression of Side reduces crawling speeds. **$P<0.01$, ***$P<0.001$ (Statistical significance calculated using two-tailed Student's *t*-test or Mann–Whitney *U*-test, compared with ShGFP control larvae). Data are mean±s.d. *n*, number of larvae; ns, not significant. Scale bars: 500 μm

of the ISNb branch (Sink et al., 2001). In addition, in *twist*-mutant embryos, which lack mesoderm-derived cells, outgrowing motor axons fail to defasciculate and do not reach the ventral body wall (Younossi-Hartenstein and Hartenstein, 1993). In contrast, individual muscle founder cells developing there spontaneously were sufficient to trigger defasciculation (Landgraf et al., 1999). Attraction to ventral muscles expressing low levels of Side when the ISNb passes this region could, therefore, be involved in triggering defasciculation.

Non-innervation of dorsal-most muscles in the ISN pathway is unlikely to arise from defasciculation defects, but could be due to growth delays. In wild-type embryos, the ISN normally grows along Side-expressing sensory axons of the dorsal cluster (Sink et al., 2001; Siebert et al., 2009), but in *side* mutants these tracks are no longer attractive. Time-lapse imaging employing a FasII-GFP exon trap showed that ISN growth rates are indeed reduced by ∼50% in *side*-mutant embryos (Siebert et al., 2009). This principle could also apply to the SNa pathway, explaining the frequent non-innervation of the distal-most muscle, M24. Thus, at endogenous levels, substrate attraction promotes axonal growth.

Endogenous Side is normally not detected in undifferentiated myoblasts. In fact, it would not make sense to attract motor axons to motile myoblasts destined for sporadic fusion events. The ISN therefore appears to largely ignore myoblasts during its dorsal migration at stages 13-15. However, upregulation of exogenous Side in these cells using Mef2-Gal4 completely re-organizes pathway decisions and innervation patterns. Too much Side deflects the ISN into false directions, causing double-headed ISNs and premature attachments to myotubes. Growth delays likely increase further because of continued cell migration in myogenic regions or because of the additional time that is required to correct misprojected nerves (retraction and regrowth). The resulting lack of dorsal NMJs is therefore caused by too much attraction but is, in principle, qualitatively similar to the lack of dorsal NMJs in *side* mutants (which is caused by too little attraction). Thus, growth delays and axonal stalls can be caused by too much or too little attraction.

As stalled growth cones have not yet formed synaptic arbours, but the embryo is in its final stages of development, with the majority of muscles already being innervated and starting active contractions, it is reasonable to ask how such growth cones develop further.
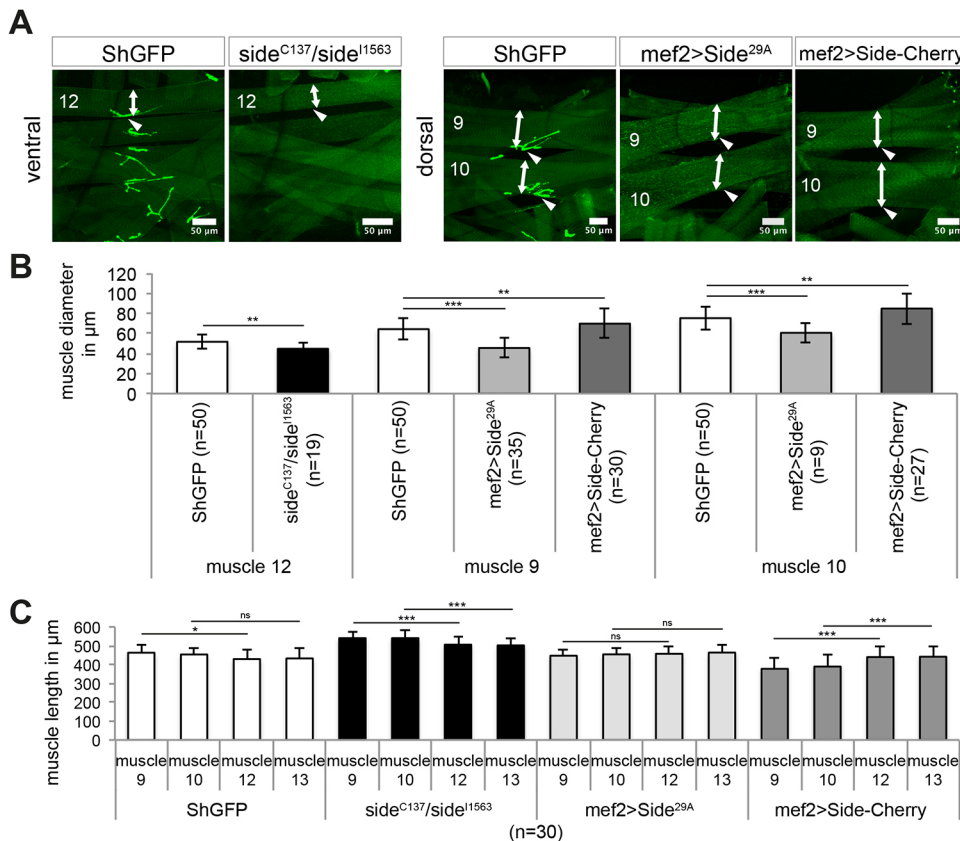
Fig. 6. Dorsal muscle thickness correlates with body curvature.
(A) Confocal images of ventral and dorsal muscle fields in third instar larvae of the indicated genotypes. Arrowheads mark the expected position of NMJs. Double-headed arrows indicate the sites and dimensions of muscle diameter measurements. Muscles 9, 10 and 12 are labelled. Genotypes: w;; ShGFP; w;; ShGFP side^{C137}/ShGFP side^{I1563}; w;; UAS-Side^{29A}/mef2-Gal4 ShGFP; w; UAS-Side-Cherry/+; mef2-Gal4 ShGFP/+. (B) Quantification of ventral and dorsal muscle diameters in the indicated genotypes. Only non-innervated muscles were evaluated in experimental genotypes. Statistical significance calculated compared with the same fibre in ShGFP larvae. (C) Lengths of dorsal and ventral muscle fibres in control and curved larvae of the indicated genotypes. Statistical significance was evaluated between M9 and M12 or M10 and M13 for each genotype. Dorsal muscles are shorter compared with ventral muscles in larvae overexpressing Side-Cherry. *$P<0.05$, **$P<0.01$, ***$P<0.001$ (statistical significance calculated using two-tailed Mann–Whitney U-test or two-tailed Student's t-test). Data are mean±s.d. n, number of muscles; ns, not significant. Scale bars: 50 μm.

Several scenarios are possible. First, they might continue to grow towards their targets and manage to establish NMJs, despite ongoing muscle movements. Second, they might not reach their targets and, instead, innervate muscle fibres nearby. Third, retractions of growth cones might trigger apoptosis in corresponding motoneurons. Because NMJs are probably unable to form on constantly contracting muscles, and as we do not find drastically reduced numbers of motoneurons in *side* mutants (data not shown), we favour the second possibility. Indeed, a subset of muscle fibres in Side loss- and gain-of-function animals are innervated at ectopic (wrong) positions, indicating that nearby muscles receive additional innervation and that compensation is possible, but only to a limited extent. Thus, axonal stalls in embryos prevent predominantly the innervation of the distal-most muscle targets of a given nerve in larvae.

It is important to emphasize that the final innervation pattern in *side* and other guidance mutants is not distributed symmetrically along and across the body axis. Although miswiring occurs in every hemisegment, the location and number of non-innervated muscles can vary greatly. Genetic mutations frequently generate symmetrical defects in bilateral animals, with only minor variations. Loss of *side*, however, results in overtly asymmetrical and unilateral phenotypes. Any ventral muscle field can range from almost normally innervated to grossly non-innervated, depending on complete or incomplete defasciculation of the ISNb/d.

One conclusion from this is that guidance decisions seem to be made rather independently in each hemisegment. Such independent nerve behaviours in adjacent hemisegments have been documented unintentionally in different mutants (Fambrough and Goodman, 1996; Mitchell et al., 1996; Desai et al., 1997; Sink et al., 2001). These observations strengthen the idea that the motor axon pattern

in *Drosophila* is not strictly hard-wired, but instead results from the cumulative integration of multiple guidance cues along a pathway (Winberg et al., 1998; Yu et al., 2000; Zarin et al., 2014a; Santiago and Bashaw, 2017). The constant summation of functionally different cues provides robustness for the guidance process, and points to a cooperative rather than a redundant mechanism (Zarin and Labrador, 2018). Eliminating a single factor then, such as Side, could destabilize the cooperation, leading to stochastic errors at various positions along a pathway.

Asymmetrical or unilateral muscle innervation due to mutations in axon guidance molecules have also been observed in mice (Helmbacher et al., 2000). During mouse hindlimb development, outgrowing motor axons migrate towards the sciatic plexus, at which point they select separating dorsal or ventral trajectories. Mutations in the tyrosine kinase receptor EphA4 lead to failures in defasciculation at this choice point, causing a striking lack of innervation of dorsal muscles, followed by hindlimb paralysis (Helmbacher et al., 2000). Of note, the penetrance of the EphA4 phenotypes correlated well with EphA4 protein levels, with heterozygous mice showing unilateral phenotypes in 30% of hindlimbs (Helmbacher et al., 2000; Chai et al., 2014).

Besides paralysis, these hindlimbs also showed clubfoot-like deformities. Clubfoot is one of the most common musculoskeletal birth defects in humans and has still uncertain aetiologies, and multiple ideas exist about its causes (Bacino and Hecht, 2014; Basit and Khoshhal, 2018). However, there is evidence that it can result from muscular or neuronal defects (Ashby et al., 1993; Ippolito et al., 2009; Alvarado et al., 2011). Our findings might therefore also help to better understand musculoskeletal or paralytic birth defects in humans. Major axon guidance errors permanently prevent the innervation of entire muscle groups, which suppresses the
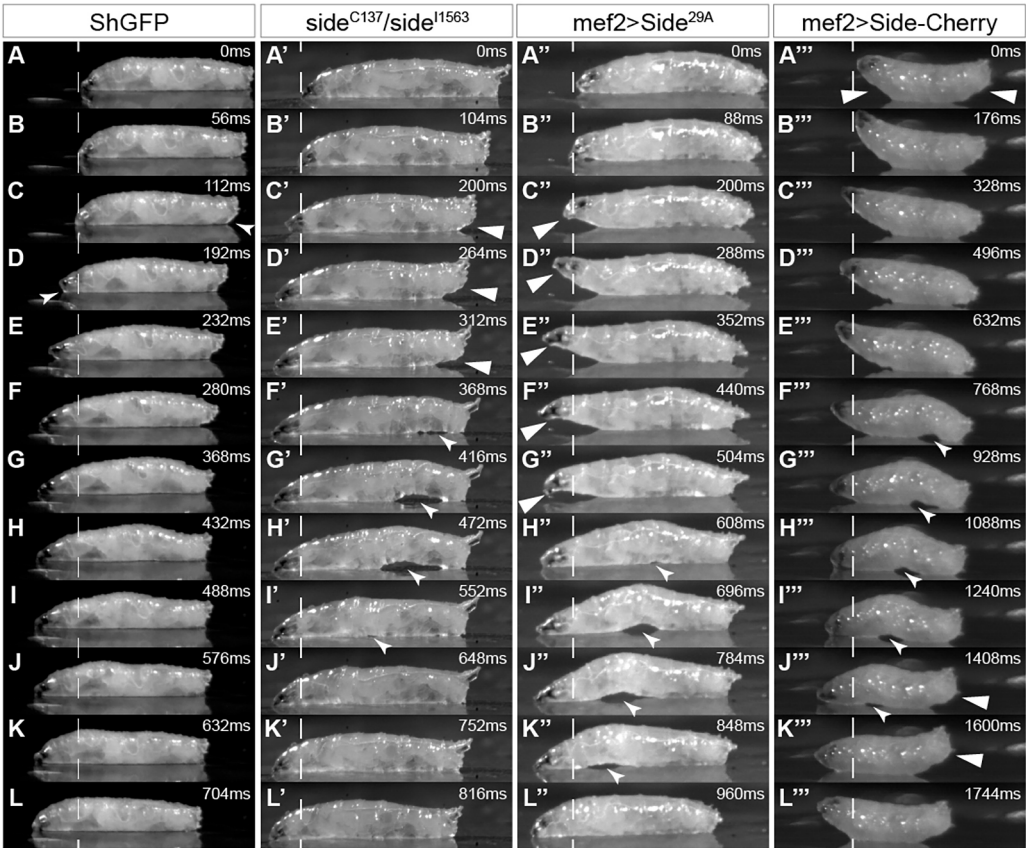
Fig. 7. High-speed videography of crawling third instar larvae reveals that axon guidance errors cause 'arching' and 'lifting' locomotion phenotypes. (A-L) Crawling pattern of ShGFP control larvae. At the start of the peristaltic wave, larvae raise their tail segment only marginally over the substrate (arrowhead in C), whereas the head maintains contact to the substrate (arrowhead in D). (A'-L') *side* mutants lift their tail segments inappropriately off the substrate (large arrowheads in C'-E'). During wave propagation, contact to the substrate is partially lost ('arching' phenotype, small arrowheads in F'-I'). (A″-L″) Larvae overexpressing untagged Side in muscles show 'arching' phenotypes (small arrowheads in H″-K″) and raise their heads and/or tails exorbitantly and for prolonged times above the substrate ('lifting' phenotype, large arrowheads in C″-G″). (A‴-L‴) Larvae overexpressing Side-Cherry in muscles show 'arching' (small arrowheads in F‴-J‴) and extreme 'lifting' phenotypes (large arrowheads in A‴,J‴-K‴). All images in this figure are taken from Movies 1-4. Dashed line indicates the position of the head at the beginning of the crawl. Genotypes: w;; ShGFP in A-L; w;; ShGFP *side*[C137]/ShGFP *side*[I1563] in A'-L'; w;; UAS-Side[29A]/mef2-Gal4 ShGFP in A″-L″; w; UAS-Side-Cherry/+; mef2-Gal4 ShGFP/+ in A‴-L‴.

execution of specific movements and/or cause deformities through unbalanced strain. Because of the stochastic behaviour of motor axons in *Drosophila*, we predict that mutations in axon guidance molecules can also cause asymmetrical innervation defects in vertebrates that are easily recognized by unilateral movements or locomotion defects.

Our movies of *side*-mutant larvae show that the basic locomotion pattern is still executed in the presence of incorrect wiring. In particular, peristaltic contraction waves seem to proceed without major interruptions, despite hemisegments lacking up to 33% of NMJs. In similar experiments, selective severing of segmental

Table 3. Quantification of larval crawling phenotypes observed in lateral and dorsal views of the indicated genotypes

Genotype	Lateral view				Dorsal view	
	n	Head lifting (%)	Tail lifting (%)	Arching (%)	n	Unbalanced (%)
ShGFP	23	35	0	0	16	6
side[C137]/*side*[I1563]	12	92	67	67	39	54
mef2>Side[29A]	19	100	47	68	18	33
mef2>Side-Cherry	38	100	84	58	7	86

n, number of larvae scored.

nerves did not prevent the propagation of peristaltic waves in the caterpillar *Manduca sexta* (Dominick and Truman, 1986). A possible reason for the persistence of segmental contractions in *Drosophila* may be that a majority of muscles are still innervated, although occasionally at unusual positions. The innervated fibres might be powerful enough to carry others along, moving them in a 'passive mode'. Longitudinal muscle fibres are all inserted at attachment sites near the segment boundary. Innervated and non-innervated longitudinal muscles are thus indirectly connected via a belt of attachment sites. Contraction of innervated dorsal muscles could, therefore, induce, at least partially, shortening of non-innervated ventral muscles in an accordion-like fashion.

Drosophila larvae are hydrostatic animals that pressurize their body cavity to antagonize muscle contractions and exert forces on the substrate (Trimmer and Lin, 2014). Using specific antibodies that recognize muscle myosin heavy chains, we were unable to detect structural abnormalities in non-innervated muscles of *side* mutants, indicating that the sarcomeric pattern is largely intact. 'Arching' and 'lifting' phenotypes therefore likely arise as a consequence of pressure differences in the haemolymph due to non-antagonized muscle contractions. In wild-type larvae, ventral and dorsal longitudinal muscles contract simultaneously, followed by transverse muscles with a short delay (out of phase contraction)

9

(Heckscher et al., 2012). If dorsal muscles are unable to contract, e.g. in animals overexpressing Side, ventral contractions might push the haemolymph into dorsal regions, increasing hydrostatic pressure there, which might lifts parts of the larvae off the substrate. Alternatively, contractions of transverse lateral muscle might suffice to detach ventral body parts from the substrate when not counterbalanced by an innervated ventral musculature. Irrespective of the exact mechanism, the movement phenotypes clearly show that embryonic axon guidance errors manifest themselves in larval locomotion defects. Together with observations that innervation patterns tend to be asymmetrical, unilateral syndromes in humans could be caused by wiring defects.

MATERIALS AND METHODS
Genetics and fly stocks
Flies were kept on standard corn meal food in yeasted vials at 25°C. The $side^{C137}$ and $side^{I1563}$ alleles were isolated in an EMS mutagenesis screen for recessive mutations affecting the structure of NMJs (Aberle et al., 2002). The side alleles were induced in a ShGFP background, therefore isogenic w^{1118};; ShGFP, insertion 7A on the third chromosome (Zito et al., 1999), was used as a control strain.

$beat^3$ (4748) and $beat^{C163}$ (4742) strains were ordered from the Bloomington Drosophila Stock Centre (BDSC). The muscle-specific driver lines Mef2-Gal4, M12-specific 5053-Gal4 and the enhancer trap line OK371-Gal4 active in glutamatergic neurons have been described (Ranganayakulu et al., 1996; Mahr and Aberle, 2006; Schnorrer et al., 2007). The following effector lines were used: UAS-Side^{29A} (Sink et al., 2001), UAS-FasciclinII (Lin and Goodman, 1994), UAS-NetrinA and B (Mitchell et al., 1996), UAS-Frazzled (Kolodziej et al., 1996), UAS-Connectin (Raghavan and White, 1997), UAS-Neuroglian^{180} (BDSC, 24169), UAS-CD4-tdTomato (Han et al., 2011) and UAS-dsRED (BDSC, 6282). To construct UAS-Side-Cherry, the full-length side cDNA (a kind gift from C.S. Goodman, UC Berkeley, CA, USA) was amplified by PCR using proofreading polymerases and cloned into the Gateway Entry Vector pENTR D-Topo (Thermo Fisher Scientific). The insert was then sequenced from both ends and inserted into the pUAST_attB_rfA-mCherry destination vector (kindly provided by Sven Bogdan, University of Münster, Germany) by LR recombination using LR clonase (Thermo Fisher Scientific). The resulting pUAST-Side-Cherry vector was integrated into the Drosophila genome using the recombination site at 51C (Bischof et al., 2007).

Immunohistochemistry
Embryos were stained as described (Mahr and Aberle, 2006). Briefly, embryos were dechorionized with 50% DanKlorix [2.8% (w/w) hypochlorite, Colgate-Palmolive], fixed with 3.7% formaldehyde in PBS and devitellinized. After rehydration using PTX (PBS+0.1% Triton X-100, Carl Roth), embryos were blocked with 5% normal goat serum (NGS, Jackson ImmunoResearch) in PTX. Incubation with primary antibodies was carried out on a nutator (VWR International) overnight at 4°C. After washing, secondary antibodies labelled with fluorescent dyes were added in PTX/NGS for 2 h at room temperature. The following primary antibodies were used: mouse anti-Fasciclin II (1D4, 1:50, Developmental Studies Hybridoma Bank) and rabbit anti-GFP (TP401, 1:1000, Acris Antibodies). Goat anti-mouse or anti-rabbit secondary antibodies conjugated with Cy3 or Alexa488, respectively (Jackson ImmunoResearch), were diluted 1:400.

Microscopy
Microscopic images were acquired on a laser scanning confocal microscope (LSM710, Carl Zeiss MicroImaging) and processed using Fiji software (Schindelin et al., 2012). Figures show maximum intensity projections of several z-sections (1024×1024 pixel, line averaging 2). Other pixel dimensions were either tile scans or image details. Third instar larvae were picked at the wandering stage, washed and immobilized by immersion in a water bath set at 60°C for 1 s. Stretched larvae were transferred to 45 µl 70% glycerol/PBS on a microscope slide. Larvae were aligned and covered by a 22×22 mm cover slide for imaging using 10×/0.45 or 20×/0.8 air objectives (Plan Apochromat, Carl Zeiss MicroImaging). Cleared embryos

were mounted in 30 µl 70% glycerol/PBS, covered with a 18×18 mm cover slide and imaged using 20×/0.8 and 40×/0.95 Corr air objectives (Plan Apochromat, Carl Zeiss Microimaging).

Quantification of axon guidance phenotypes
Innervation phenotypes were quantified in intact third instar larvae using the postsynaptic NMJ marker ShGFP (Zito et al., 1999). ShGFP reliably stains NMJs forming type I boutons and indirectly reflects motor nerve projections, as postsynaptic terminals develop only upon innervation at the nerve entry point (Meyer and Aberle, 2006). The locations of NMJs were evaluated in up to four abdominal hemisegments (A2-A6) per larva, using confocal image stacks that were acquired (1024×1024 pixel, line averaging 2, tile scan 1-2 length×4-5 width) on a confocal laser scanning microscope (TCS SP8, Leica Microsystems) using a 10×/0.3 air objective (HC PL Fluotar) imported in Fiji (Schindelin et al., 2012). Each hemisegment was divided into a dorsal muscle field (muscles 1, 2, 9, 10, 18), lateral muscle field (muscles 3, 4, 5, 8, 11, 19, 20, 21, 22, 23, 24) and ventral muscle field (muscles 6, 7, 12, 13, 14, 15, 16, 17, 26, 27, 28, 29, 30). NMJs were counted using the multi-point tool in Fiji. Muscle diameter and length were determined using the straight line tool in Fiji.

Statistical analysis
All statistical graphics display the mean and standard deviation (s.d.) of the individual parameters using Microsoft Excel. Datasets were tested for normal distribution using the Kolmogorov–Smirnov test with Lilliefors correction. P-values were determined using a two-tailed Student's t-test for normal distributed datasets, or were calculated using a two-tailed Mann–Whitney U-test for not normal distributed datasets (***$P \leq 0.001$, **$P \leq 0.01$, *$P \leq 0.05$, ns=not significant).

Larval locomotion assay
First (28-36 h after egg laying) or third (wandering stage) instar larvae were picked using spring steel tweezers and cleaned with tap water to remove putative food and yeast particles. For each experiment, two larvae were placed on apple juice agar plates (35 mm diameter×13 mm height) adapted to room temperature. Larval crawling was recorded for 1 min (third instar larvae) or 10 min (first instar larvae) at 0.5 or 2 frames per second, respectively, using a DS-Qi2 monochrome microscope camera (Nikon) mounted on a SMZ25 stereomicroscope (Nikon) equipped with a P2-SHR Plan Apo 0.5× objective (Nikon). Images were imported into Fiji (Schindelin et al., 2012) and quantified using the z-projection function and the freehand line tool.

Videography
High-speed movies of crawling third instar larvae were collected using a 1.3 megapixel high-speed imaging camera [Photron Fastcam Mini UX100 (Model 800K/M1), VKT] equipped with a macro zoom lens (Computar macro zoom 0.3×, 1:4.5 coupled with a Cosmicar/Pentax X2 Extender). Larvae were recorded from dorsal and lateral views at 125 frames per second during crawling, on a 2% agarose block stained with bromophenol blue (~ 0.01%, Carl Roth). Images were saved on a Lenovo 2447/W530 notebook and processed with Photron Fastcam Viewer software (version 3.52; VKT) for data export to an iMac (Apple). Biometry for quantitative crawling behaviour was analyzed using VCode/VData software (version 1.2) (Hagedorn et al., 2008). Duration of a peristaltic wave was measured as the time interval between the first and last contracting segments, in a posterior to anterior direction. Time series were assembled and edited using Fiji software (Schindelin et al., 2012).

Asymmetry in muscle contraction was evaluated in dorsal views according to previous findings (Heckscher et al., 2015). Briefly, movies of third instar larvae were collected at 50 fps using the Photron high-speed camera mounted on an Axio Imager M2 microscope (Carl Zeiss MicroImaging) equipped with a N-Achroplan 10×/0.25 objective. Living larvae were placed in 60-80 µl 70% glycerol/PBS on microscope slides and covered with 18×18 mm cover slides. After videography, larvae were imaged using the LSM710 confocal microscope to identify segments with asymmetrical innervation. Maximal muscle contraction was analysed manually using the straight line tool in Fiji for three to five contractions

for each larva. For control larvae (ShGFP), right and left hemisegments of the abdominal segments A3 or A4 were analysed. For quantification of *side*-mutant larvae, only those larvae that lacked innervation on ventral muscles in at least three consecutive hemisegments were considered. Well innervated sides of the body were distinguished from less well innervated sides (A3 to A5). Only one or two segments per larva were measured for both genotypes.

Competing interests
The authors declare no competing or financial interests.

Author contributions
Methodology: J.C.K.; Data curation: J.C.K., C.P.; Visualization: J.C.K., C.P.; Supervision: H.A.; Project administration: H.A.; Funding acquisition: H.A.

Supplementary information
Supplementary information available online at
http://dev.biologists.org/lookup/doi/10.1242/dev.163279.supplemental

References
Aberle, H. (2009). Searching for guidance cues: follow the Sidestep trail. *Fly* **3**, 270-273.

Aberle, H., Haghighi, A. P., Fetter, R. D., McCabe, B. D., Magalhães, T. R. and Goodman, C. S. (2002). wishful thinking encodes a BMP type II receptor that regulates synaptic growth in Drosophila. *Neuron* **33**, 545-558.

Ainsley, J. A., Pettus, J. M., Bosenko, D., Gerstein, C. E., Zinkevich, N., Anderson, M. G., Adams, C. M., Welsh, M. J. and Johnson, W. A. (2003). Enhanced locomotion caused by loss of the Drosophila DEG/ENaC protein Pickpocket1. *Curr. Biol.* **13**, 1557-1563.

Alvarado, D. M., McCall, K., Aferol, H., Silva, M. J., Garbow, J. R., Spees, W. M., Patel, T., Siegel, M., Dobbs, M. B. and Gurnett, C. A. (2011). Pitx1 haploinsufficiency causes clubfoot in humans and a clubfoot-like phenotype in mice. *Hum. Mol. Genet.* **20**, 3943-3952.

Araújo, S. J. and Tear, G. (2003). Axon guidance mechanisms and molecules: lessons from invertebrates. *Nat. Rev. Neurosci.* **4**, 910-922.

Ashby, P. R., Wilson, S. J. and Harris, A. J. (1993). Formation of primary and secondary myotubes in aneural muscles in the mouse mutant peroneal muscular atrophy. *Dev. Biol.* **156**, 519-528.

Bacino, C. A. and Hecht, J. T. (2014). Etiopathogenesis of equinovarus foot malformations. *Eur. J. Med. Genet.* **57**, 473-479.

Basit, S. and Khoshhal, K. I. (2018). Genetics of clubfoot; recent progress and future perspectives. *Eur. J. Med. Genet.* **61**, 107-113.

Berrigan, D. and Pepin, D. J. (1995). How maggots move: Allometry and Kinematics of crawling in larval diptera. *J. Insect Physiol.* **41**, 329-337.

Bischof, J., Maeda, R. K., Hediger, M., Karch, F. and Basler, K. (2007). An optimized transgenesis system for Drosophila using germ-line-specific phiC31 integrases. *Proc. Natl. Acad. Sci. USA* **104**, 3312-3317.

Chai, G., Zhou, L., Manto, M., Helmbacher, F., Clotman, F., Goffinet, A. M. and Tissir, F. (2014). Celsr3 is required in motor neurons to steer their axons in the hindlimb. *Nat. Neurosci.* **17**, 1171-1179.

de Jong, S., Cavallo, J. A., Rios, C. D., Dworak, H. A. and Sink, H. (2005). Target recognition and synaptogenesis by motor axons: responses to the sidestep protein. *Int. J. Dev. Neurosci.* **23**, 397-410.

Desai, C. J., Krueger, N. X., Saito, H. and Zinn, K. (1997). Competition and cooperation among receptor tyrosine phosphatases control motoneuron growth cone guidance in Drosophila. *Development* **124**, 1941-1952.

Dixit, R., Vijayraghavan, K. and Bate, M. (2008). Hox genes and the regulation of movement in Drosophila. *Dev. Neurobiol.* **68**, 309-316.

Dobi, K. C., Schulman, V. K. and Baylies, M. K. (2015). Specification of the somatic musculature in Drosophila. *Wiley Interdiscip. Rev. Dev. Biol.* **4**, 357-375.

Dominick, O. S. and Truman, J. W. (1986). The physiology of wandering behaviour in Manduca sexta. III. Organization of wandering behaviour in the larval nervous system. *J. Exp. Biol.* **121**, 115-132.

Fambrough, D. and Goodman, C. S. (1996). The Drosophila beaten path gene encodes a novel secreted protein that regulates defasciculation at motor axon choice points. *Cell* **87**, 1049-1058.

Green, C. H., Burnet, B. and Connolly, K. J. (1983). Organization and patterns of inter- and intraspecific variation in the behaviour of Drosophila larvae. *Anim. Behav.* **31**, 282-291.

Hagedorn, J., Hailpern, J. and Karahalios, K. G. (2008). VCode and VData: Illustrating a new framework for supporting the video annotation workflow. In *Proceedings of the Working Conference on Advanced Visual Interfaces (AVI '08)*, pp.317-321.

Han, C., Jan, L. Y. and Jan, Y.-N. (2011). Enhancer-driven membrane markers for analysis of nonautonomous mechanisms reveal neuron-glia interactions in Drosophila. *Proc. Natl. Acad. Sci. USA* **108**, 9673-9678.

Heckscher, E. S., Lockery, S. R. and Doe, C. Q. (2012). Characterization of Drosophila larval crawling at the level of organism, segment, and somatic body wall musculature. *J. Neurosci.* **32**, 12460-12471.

Heckscher, E. S., Zarin, A. A., Faumont, S., Clark, M. Q., Manning, L., Fushiki, A., Schneider-Mizell, C. M., Fetter, R. D., Truman, J. W., Zwart, M. F. et al. (2015). Even-Skipped(+) interneurons are core components of a sensorimotor circuit that maintains left-right symmetric muscle contraction amplitude. *Neuron* **88**, 314-329.

Helmbacher, F., Schneider-Maunoury, S., Topilko, P., Tiret, L. and Charnay, P. (2000). Targeting of the EphA4 tyrosine kinase receptor affects dorsal/ventral pathfinding of limb motor axons. *Development* **127**, 3313-3324.

Ippolito, E., De Maio, F., Mancini, F., Bellini, D. and Orefice, A. (2009). Leg muscle atrophy in idiopathic congenital clubfoot: is it primitive or acquired? *J. Child. Orthop.* **3**, 171-178.

Kolodkin, A. L. and Tessier-Lavigne, M. (2011). Mechanisms and molecules of neuronal wiring: a primer. *Cold Spring Harb. Perspect. Biol.* **3**, a001727.

Kolodziej, P. A., Timpe, L. C., Mitchell, K. J., Fried, S. R., Goodman, C. S., Jan, L. Y. and Jan, Y. N. (1996). frazzled encodes a Drosophila member of the DCC immunoglobulin subfamily and is required for CNS and motor axon guidance. *Cell* **87**, 197-204.

Labrador, J. P., O'Keefe, D., Yoshikawa, S., McKinnon, R. D., Thomas, J. B. and Bashaw, G. J. (2005). The homeobox transcription factor even-skipped regulates netrin-receptor expression to control dorsal motor-axon projections in Drosophila. *Curr. Biol.* **15**, 1413-1419.

Landgraf, M., Baylies, M. and Bate, M. (1999). Muscle founder cells regulate defasciculation and targeting of motor axons in the Drosophila embryo. *Curr. Biol.* **9**, 589-592.

Li, H., Watson, A., Olechwier, A., Anaya, M., Sorooshyari, S. K., Harnett, D. P., Lee, H. P., Vielmetter, J., Fares, M. A., Garcia, K. C. et al. (2017). Deconstruction of the Beaten path-Sidestep interaction network provides insights into neuromuscular system development. *eLife* **6**, e28111.

Lin, D. M. and Goodman, C. S. (1994). Ectopic and increased expression of Fasciclin II alters motoneuron growth cone guidance. *Neuron* **13**, 507-523.

Mahr, A. and Aberle, H. (2006). The expression pattern of the Drosophila vesicular glutamate transporter: a marker protein for motoneurons and glutamatergic centers in the brain. *Gene Expr. Patterns* **6**, 299-309.

Meyer, F. and Aberle, H. (2006). At the next stop sign turn right: the metalloprotease Tolloid-related 1 controls defasciculation of motor axons in Drosophila. *Development* **133**, 4035-4044.

Mitchell, K. J., Doyle, J. L., Serafini, T., Kennedy, T. E., Tessier-Lavigne, M., Goodman, C. S. and Dickson, B. J. (1996). Genetic analysis of Netrin genes in Drosophila: Netrins guide CNS commissural axons and peripheral motor axons. *Neuron* **17**, 203-215.

Nose, A., Takeichi, M. and Goodman, C. S. (1994). Ectopic expression of connectin reveals a repulsive function during growth cone guidance and synapse formation. *Neuron* **13**, 525-539.

Özkan, E., Carrillo, R. A., Eastman, C. L., Weiszmann, R., Waghray, D., Johnson, K. G., Zinn, K., Celniker, S. E. and Garcia, K. C. (2013). An extracellular interactome of immunoglobulin and LRR proteins reveals receptor-ligand networks. *Cell* **154**, 228-239.

Pipes, G. C., Lin, Q., Riley, S. E. and Goodman, C. S. (2001). The Beat generation: a multigene family encoding IgSF proteins related to the Beat axon guidance molecule in Drosophila. *Development* **128**, 4545-4552.

Raghavan, S. and White, R. A. H. (1997). Connectin mediates adhesion in Drosophila. *Neuron* **18**, 873-880.

Ranganayakulu, G., Schulz, R. A. and Olson, E. N. (1996). Wingless signaling induces nautilus expression in the ventral mesoderm of the Drosophila embryo. *Dev. Biol.* **176**, 143-148.

Risse, B., Thomas, S., Otto, N., Löpmeier, T., Valkov, D., Jiang, X. and Klämbt, C. (2013). FIM, a novel FTIR-based imaging method for high throughput locomotion analysis. *PLoS ONE* **8**, e53963.

Roberts, M. J. (1971). On the locomotion of cyclorrhaphan maggots (Diptera). *J. Nat. Hist.* **5**, 583-590.

Santiago, C. and Bashaw, G. J. (2017). Islet coordinately regulates motor axon guidance and dendrite targeting through the Frazzled/DCC receptor. *Cell Rep.* **18**, 1646-1659.

DEVELOPMENT

Schindelin, J., Arganda-Carreras, I., Frise, E., Kaynig, V., Longair, M., Pietzsch, T., Preibisch, S., Rueden, C., Saalfeld, S., Schmid, B. et al. (2012). Fiji: an open-source platform for biological-image analysis. *Nat. Methods* **9**, 676-682.

Schnorrer, F., Kalchhauser, I. and Dickson, B. J. (2007). The transmembrane protein Kon-tiki couples to Dgrip to mediate myotube targeting in Drosophila. *Dev. Cell* **12**, 751-766.

Shishido, E., Takeichi, M. and Nose, A. (1998). Drosophila synapse formation: regulation by transmembrane protein with Leu-rich repeats, CAPRICIOUS. *Science* **280**, 2118-2121.

Siebert, M., Banovic, D., Goellner, B. and Aberle, H. (2009). Drosophila motor axons recognize and follow a Sidestep-labeled substrate pathway to reach their target fields. *Genes Dev.* **23**, 1052-1062.

Sink, H., Rehm, E. J., Richstone, L., Bulls, Y. M. and Goodman, C. S. (2001). sidestep encodes a target-derived attractant essential for motor axon guidance in Drosophila. *Cell* **105**, 57-67.

Suster, M. L., Martin, J.-R., Sung, C. and Robinow, S. (2003). Targeted expression of tetanus toxin reveals sets of neurons involved in larval locomotion in Drosophila. *J. Neurobiol.* **55**, 233-246.

Trimmer, B. A. and Lin, H.-T. (2014). Bone-free: soft mechanics for adaptive locomotion. *Integr. Comp. Biol.* **54**, 1122-1135.

Wang, J. W., Sylwester, A. W., Reed, D., Wu, D.-A. J., Soll, D. R. and Wu, C.-F. (1997). Morphometric description of the wandering behavior in Drosophila larvae: aberrant locomotion in Na+ and K+ channel mutants revealed by computer-assisted motion analysis. *J. Neurogenet.* **11**, 231-254.

Weitkunat, M. and Schnorrer, F. (2014). A guide to study Drosophila muscle biology. *Methods* **68**, 2-14.

Winberg, M. L., Mitchell, K. J. and Goodman, C. S. (1998). Genetic analysis of the mechanisms controlling target selection: complementary and combinatorial functions of netrins, semaphorins, and IgCAMs. *Cell* **93**, 581-591.

Younossi-Hartenstein, A. and Hartenstein, V. (1993). The role of the tracheae and musculature during pathfinding of Drosophila embryonic sensory axons. *Dev. Biol.* **158**, 430-447.

Yu, H. H., Huang, A. S. and Kolodkin, A. L. (2000). Semaphorin-1a acts in concert with the cell adhesion molecules fasciclin II and connectin to regulate axon fasciculation in Drosophila. *Genetics* **156**, 723-731.

Zarin, A. A. and Labrador, J. -P. (2017). Motor axon guidance in Drosophila. *Semin. Cell Dev. Biol.* (in press).

Zarin, A. A., Asadzadeh, J., Hokamp, K., McCartney, D., Yang, L., Bashaw, G. J. and Labrador, J.-P. (2014a). A transcription factor network coordinates attraction, repulsion, and adhesion combinatorially to control motor axon pathway selection. *Neuron* **81**, 1297-1311.

Zarin, A. A., Asadzadeh, J. and Labrador, J.-P. (2014b). Transcriptional regulation of guidance at the midline and in motor circuits. *Cell. Mol. Life Sci.* **71**, 419-432.

Zinn, K. (2009). Choosing the road less traveled by: a ligand-receptor system that controls target recognition by Drosophila motor axons. *Genes Dev.* **23**, 1042-1045.

Zito, K., Parnas, D., Fetter, R. D., Isacoff, E. Y. and Goodman, C. S. (1999). Watching a synapse grow: noninvasive confocal imaging of synaptic growth in Drosophila. *Neuron* **22**, 719-729.